

VIP Very Important Paper

Special  
Collection

# High Cycling Stability for Solid-State Li Metal Batteries via Regulating Solvation Effect in Poly(Vinylidene Fluoride)-Based Electrolytes

Xue Zhang,<sup>[a]</sup> Jian Han,<sup>[a]</sup> Xiangfu Niu,<sup>[b]</sup> Chengzhou Xin,<sup>[a]</sup> Chuanjiao Xue,<sup>[a]</sup> Shuo Wang,<sup>[a]</sup> Yang Shen,<sup>[a]</sup> Liang Zhang,<sup>[b, c]</sup> Liangliang Li,<sup>\*[a]</sup> and Ce-Wen Nan<sup>\*[a]</sup>

Solid polymer electrolytes have emerged as promising alternatives to current liquid electrolytes due to their advantages in battery safety and stability. Among various polymer electrolytes, poly(vinylidene fluoride) (PVDF)-based electrolytes with high ionic conductivity, large mechanical strength, and excellent electrochemical and thermal stability have a great potential for practical applications. However, fundamental issues, such as how the Li ions transport in the PVDF-based electrolytes and how the residual solvent affects the cell performance, are unclear. Here, we demonstrate that the solvation effect due to a small amount of residual *N,N*-dimethylformamide (DMF) bound into the electrolytes plays a critical role in ionic transport, interface stability, and cell performance. With the residual DMF existing in the electrolytes in a bound state not as free solvent, the ionic conduction could be realized by the Li-ion transport among the interaction sites between the bound DMF and PVDF chains. Regulating the solvation effect in the electrolytes can make the PVDF-based solid-state Li metal batteries a significantly improved cycling performance at 25 °C (e.g., over 1000 cycles with a capacity retention of more than 94%). These findings would promote the development of next-generation Li metal batteries with high energy density and safety.

Lithium (Li)-ion batteries are pervasively used for portable electronics, large-scale power sources driving electric automobiles and power grid systems.<sup>[1]</sup> High energy density and safety are two critical features for practical Li-ion batteries.<sup>[2]</sup> Utilizing a high capacity cathode (e.g., Ni-rich NCMs [ $\text{Li}_{1+y-z}\text{Co}_y\text{Mn}_{z-1-y}\text{O}_2$ ], S and O<sub>2</sub>) with a Li metal anode can effectively increase the battery energy density.<sup>[3]</sup> However,

many challenges emerge when current organic liquid electrolytes are used in these Li metal batteries in regard to the battery performance and safety. For example, the electrochemical oxidation of organic liquid electrolytes causes the gas evolution in Li–NCM batteries.<sup>[4]</sup> Dissolution of polysulfide in organic liquid electrolytes can lead to the shuttle effect and accelerate the capacity fading of Li–S batteries.<sup>[5]</sup> Chemically unstable liquid electrolytes can also result in a poor cycling performance and limited rate capability of Li–O<sub>2</sub> batteries.<sup>[6]</sup> In addition, the uncontrolled Li dendrite growth in liquid Li metal batteries can penetrate through the separator, leading to a short circuit and eventually a fire in the battery cells due to the flammability and volatility nature of liquid electrolytes.<sup>[7]</sup>

To address the aforementioned issues, solid polymer electrolytes are developed due to their improved safety and electrochemical stability versus the liquid counterparts.<sup>[8]</sup> Polymer electrolytes are very promising to be used in commercial Li-ion batteries, due to light weight, easy processability and scalability, and low manufacturing cost. Up to now, various polymers such as polyethylene oxide (PEO), polyacrylonitrile (PAN), poly(propylene carbonate) (PPC) and poly(vinylidene fluoride) (PVDF) have been used as matrixes in polymer electrolytes.<sup>[9]</sup> Among these polymers, PVDF is being widely studied. In many cases, PVDF is recognized just as the polymer skeleton in gel electrolytes, i.e., the porous PVDF skeleton synthesized by phase inversion or electrospinning soaks a large amount of free liquid electrolyte (usually, >50 wt.%).<sup>[10]</sup> The gel electrolytes with a high uptake of free liquid electrolytes show high ionic conductivity due to fast Li-ion transport as in the liquid electrolytes, but they still have safety hazards like liquid electrolytes. Besides gel electrolytes, dry solid electrolytes based on PVDF have been obtained without free liquid electrolytes,<sup>[11,12]</sup> which show a significant improvement in the mechanical strength and safety versus the wet gel electrolytes. In comparison with other reported solid polymer electrolytes such as the mostly studied PEO-based electrolytes, such PVDF-based electrolytes have higher ionic conductivity, better thermostability and larger mechanical strength.<sup>[12,13]</sup> The PVDF-based electrolytes with superior overall performance hence have a great potential in practical applications. To date, most of studies on PVDF-based solid electrolytes have been focused on the improvement of the electrochemical performance by incorporating additives like inorganic fillers.<sup>[12–14]</sup> However, the fundamental issues such as the ionic transport in the PVDF-based electrolytes and the interface chemistry between the

[a] X. Zhang, J. Han, C. Xin, C. Xue, S. Wang, Prof. Y. Shen, Prof. L. Li, Prof. C.-W. Nan

State Key Laboratory of New Ceramics and Fine Processing  
School of Materials Science and Engineering  
Tsinghua University, Beijing 100084, China  
E-mail: liangliang@tsinghua.edu.cn  
cwnan@tsinghua.edu.cn

[b] X. Niu, Prof. L. Zhang  
School of Vehicle and Mobility  
Tsinghua University, Beijing 100084, China

[c] Prof. L. Zhang  
Center for Combustion Energy  
Tsinghua University, Beijing 100084, China

 Supporting information for this article is available on the WWW under  
<https://doi.org/10.1002/batt.202000081>

 An invited contribution to a Special Collection on Lithium Metal Anode Processing and Interface Engineering

electrolytes and electrodes, which are critical to the long-term cycling stability of the electrolytes in full cells, are unclear.

It has been found that a small amount of *N,N*-dimethylformamide (DMF) remains in the PVDF-based electrolytes if DMF is used as solvent in the preparation of the electrolytes. DMF can help to increase the ionic conductivity of the PVDF-based electrolytes as reported by Yao et al.<sup>[13]</sup> DMF is also critical to the interface stability between electrolytes and electrodes, because it can be employed as an electrophilic or nucleophilic agent that participates in reactions.<sup>[15]</sup> For example, a PVDF-DMF solution can react with Li metal to form a stable LiF layer that reduces the interfacial reactions between the electrolyte and a Li anode.<sup>[16]</sup> At a large current density, DMF may be relevant to the thickening of the interface layer between PVDF-based electrolytes and Li metal.<sup>[11]</sup> Nevertheless, the specific effect of DMF on the ionic transport in PVDF-based electrolytes and the evolution of the electrolyte-electrode interface are still not clear.

In this work, the role of residual DMF in the PVDF-based electrolytes was investigated via systematic experiments combined with first-principles calculations. We elucidated the interactions among Li salt, DMF and PVDF chains in the electrolytes and a possible ionic transport mechanism in the PVDF-based solid electrolytes. We investigated the chemical reactions induced by the residual DMF, which significantly affects the electrochemical stability of the electrolytes. By controlling the solvation effect caused by DMF, the PVDF-based electrolyte with high ionic conductivity, wide electrochemical window and excellent stability against a Li anode delivers a

significantly improved cycling performance in a Li metal full cell.

PVDF-LiN(SO<sub>2</sub>F)<sub>2</sub> (LiFSI) electrolyte membranes were prepared via a solution-casting method with DMF or tetrahydrofuran (THF)-DMF as solvent as before.<sup>[11,12]</sup> It is hard to completely remove the DMF in as-prepared electrolyte membranes, as evidenced by the weight loss before 153 °C in the thermogravimetry analysis (TGA) curves of the electrolytes (Figure S1a) and the detected peaks at 165.1, 37.5 and 32.1 ppm in the solid-state nuclear magnetic resonance (ss-NMR) spectra of the electrolytes (Figure S1b). The amount of residual DMF in the electrolytes is determined by gas chromatography (GC) and NMR methods and the details are shown in Note S1 in Supporting Information. According to the amount of residual DMF, as-prepared PVDF-LiFSI electrolyte membranes can be divided into three categories, i.e., high DMF content (14–17 wt. %), medium DMF content (10–14 wt.%) and low DMF content (5–10 wt.%), hereinafter referred to as “high-DMF electrolyte”, “medium-DMF electrolyte” and “low-DMF electrolyte”, respectively. Figure 1a compares the ionic conductivity of the high-, medium- and low-DMF electrolytes at room temperature. The average ionic conductivity is  $1.3 \times 10^{-4} \text{ Scm}^{-1}$  at 25 °C for the high-DMF electrolyte, which is the highest, and it decreases with the decrease of the DMF content. Arrhenius plots in Figure 1b further show that the activation barrier for Li<sup>+</sup> transport is the lowest in the high-DMF electrolyte and the highest in the low-DMF electrolyte. The DMF residue can affect the structure of the PVDF-based electrolytes and thus the conduction of Li<sup>+</sup> in the electrolytes. The FTIR spectra in

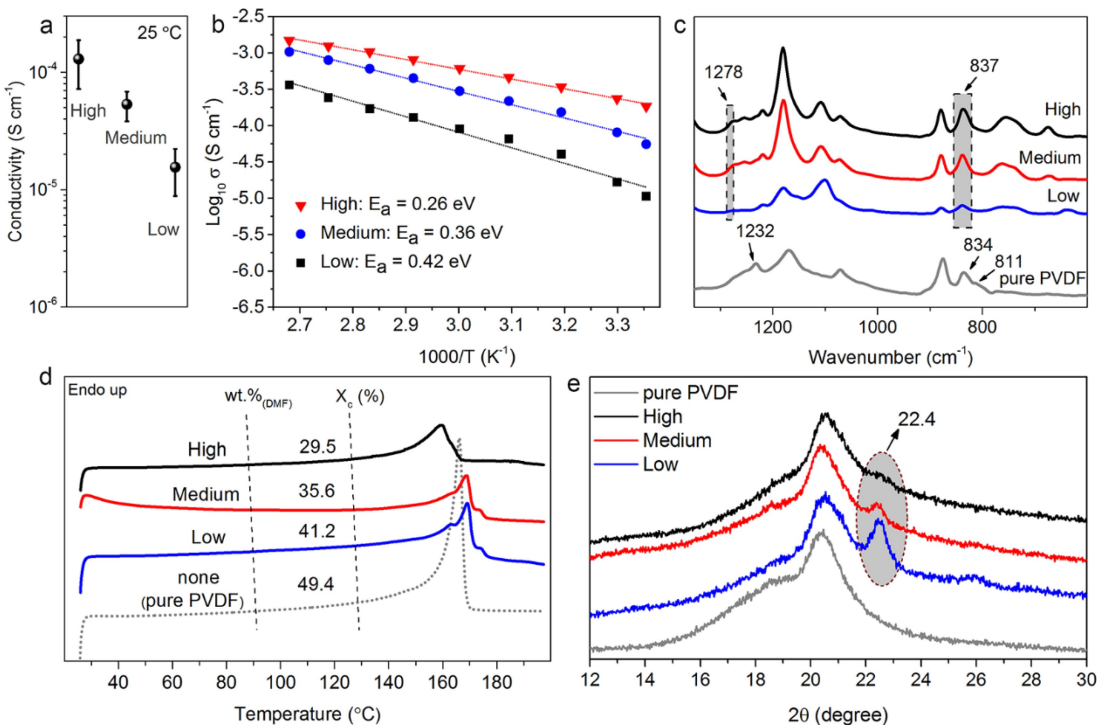


**Figure 1.** Effects of residual DMF on ionic conduction in PVDF-LiFSI electrolytes: a) ionic conductivity (25 °C) and b) Arrhenius plots of the high-, medium- and low-DMF electrolytes. Comparison of c) FTIR spectra, d) DSC melting behaviors, and e) XRD patterns, for pure PVDF film, and high-, medium- and low-DMF electrolytes.

Figure 1c indicate the existence of  $\beta$ -phase PVDF in as-prepared PVDF–LiFSI electrolyte membranes but  $\gamma$ -phase PVDF in as-prepared pure PVDF membrane, as evidenced by the corresponding characteristic peaks at 837 and 1278  $\text{cm}^{-1}$  and 811, 834, and 1232  $\text{cm}^{-1}$ , respectively.<sup>[17]</sup> The differential scanning calorimetry (DSC) analysis in Figure 1d further demonstrates that the crystallinity of PVDF decreases with the increase of the DMF content. In addition, the PVDF–LiFSI electrolyte with a high content of DMF (14–17 wt.%) has a high solubility of LiFSI, which is confirmed by the X-ray diffraction (XRD) patterns in Figure 1e. As is shown, the peak at 22.4°, which is ascribed to LiFSI as demonstrated in Figure S3, decreases with the increase of the DMF content.

To shed more light on the Li-ion transport mechanism in the electrolytes, the status of the residual DMF in the PVDF–LiFSI electrolytes was further investigated. Without Li salt added, DMF can be easily removed from the pure PVDF films under vacuum even at 40°C in spite of a high boiling point of 153°C for DMF (Figure S1). Thus, it can be inferred that the residual DMF in the PVDF-based electrolytes may strongly interact with Li salt. To figure out the interplay between DMF and Li salt, the FTIR spectra of LiFSI in the DMF solutions with different salt concentrations were recorded and summarized in the upper part of Figure 2a. The FTIR band at 658  $\text{cm}^{-1}$  is assigned to the O=C–N bending of free DMF.<sup>[18]</sup> With the increase of the LiFSI concentration, the peak related to free DMF gradually decreases and a new band at 673  $\text{cm}^{-1}$  shows up. This new band is attributed to the DMF bound to  $\text{Li}^+$  or DMF solvating  $\text{Li}^+$ .<sup>[18,19]</sup> The solvation number is calculated to be

3.29 based on the curve-fitting analysis of the FTIR spectra (see Figure S4), which means that DMF can solvate  $\text{Li}^+$  to form  $[\text{Li}(\text{DMF})_{3.29}]^+$  complex in the DMF–LiFSI solutions. Of particular interest to note is that the band for free DMF disappears, but only the band for the bound DMF exists in the FTIR spectra for the PVDF–LiFSI electrolytes as presented in the lower part of Figure 2a. When the time of vacuum drying in the electrolyte preparation increases from 16 to 33 h, the intensity of the band for the bound DMF decreases due to decrease in the amount of residual DMF. Therefore, all of residual DMF molecules in the high-, medium-, and low-DMF electrolytes are bound to  $\text{Li}^+$  with a complex form of  $[\text{Li}(\text{DMF})_x]^+$  ( $x \leq 3.29$ ), and there is no free DMF solvent in the electrolytes. This conclusion is also confirmed by the Raman spectra in Figure S5. Furthermore, the FTIR spectra in Figure 2b show that the peaks between 860 and 890  $\text{cm}^{-1}$  change with PVDF dissolved in DMF, which demonstrates some interaction between the PVDF chains and DMF.<sup>[18]</sup> To further understand the interactions between Li, DMF and PVDF in the PVDF-based electrolyte system, density functional theory (DFT) calculations with Van der Walls correction were performed. According to the experimentally fitted solvation number above, the Li–DMF complex is modeled as three DMF molecules coordinating with one Li in a planar triangle geometry for simplicity, as shown in Figure S6a. The DFT calculations gave an accumulative binding energy of –2.45 eV between Li and three DMFs (0.816 eV per Li–O in average), and a much smaller binding energy of –0.51 eV between the Li–DMF complex and the PVDF chain (Figure S6b).

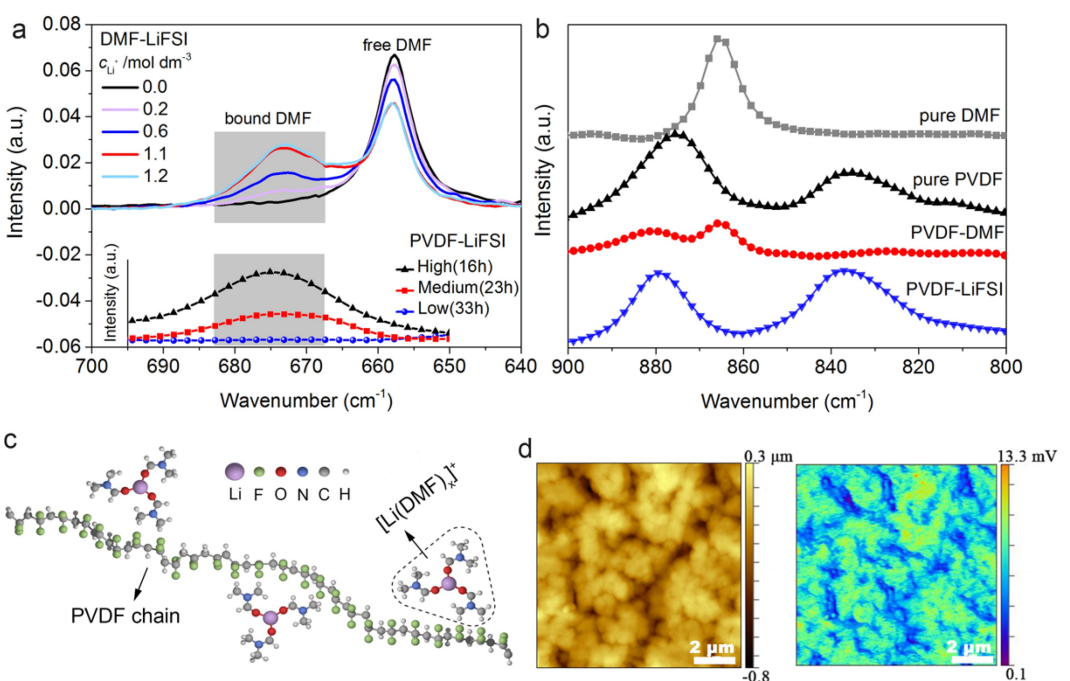


**Figure 2.** Chemical structure of DMF in PVDF-based electrolytes. a) FTIR spectra in the range of 640–700  $\text{cm}^{-1}$  observed for DMF–LiFSI solutions with various salt concentrations ( $c_{\text{Li}} = 0.0\text{--}1.2 \text{ mol dm}^{-3}$ ), and high-, medium- and low-DMF electrolyte membranes prepared with different vacuum drying time (16–33 h). b) FTIR spectra of pure DMF, pure PVDF, a PVDF–DMF solution and PVDF–LiFSI electrolyte in the range of 800–900  $\text{cm}^{-1}$ . c) A simple schematic diagram of the structure of  $[\text{Li}(\text{DMF})_x]^+$  ( $x \leq 3.29$ ) in the PVDF–LiFSI electrolyte. d) NanolR investigation. The left is the height map of a PVDF–LiFSI electrolyte film and the right is the corresponding IR intensity map of C=O vibration of DMF at 1670  $\text{cm}^{-1}$ .

Based on the analysis above, a schematic diagram of the structure of the residual DMF in the PVDF–LiFSI electrolyte is depicted in Figure 2c. Nanoscale infrared spectroscopy (nanolIR) maps in Figure 2d show that the bound DMF is uniformly distributed in the electrolytes. Thus in the electrolytes, all of residual DMF molecules are bound to Li ions to form  $[\text{Li}(\text{DMF})_x]^+$ , and then the bound DMF molecules weakly interact with PVDF chains again. With no support of free solvent,  $\text{Li}^+$  could be transported, with the assistance of PVDF chains, among the interaction sites between  $[\text{Li}(\text{DMF})_x]^+$  and the PVDF chains, which would be analogous to that in PEO-based solid electrolytes where Li ions are migrated among the O–Li interaction sites.<sup>[20]</sup> As discussed above, the residual DMF can facilitate the dissolution of Li salt into the electrolytes (Figure 1e) and increase the flexibility of PVDF chains via a plasticizing effect (Figure 1d). Therefore, for the high-, medium- and low-DMF electrolytes, the electrolyte with more DMF residue has a higher concentration of  $[\text{Li}(\text{DMF})_x]^+$  and a lower activation barrier for ionic migration, and thus higher ionic conductivity. As noted, however, this is a possible explanation, and future studies seem warranted to fully understand the Li-ion transport mechanism in the electrolytes.

In order to investigate the effect of the residual DMF on the electrochemical stability of the PVDF-based electrolytes, the symmetric cells with the PVDF–LiFSI electrolytes sandwiched between two Li foils were assembled and periodically cycled by charging/discharging for 0.5 h at a current density of  $0.5 \text{ mA cm}^{-2}$ . As shown in Figure 3a, the cycling life of the Li|Li cells gradually increases with the increase of the drying time that corresponds to the decrease of DMF residue in the electrolytes. The medium-DMF electrolyte shows better electro-

chemical stability against Li metal in comparison with the high-DMF electrolyte, which is also demonstrated by the Weibull plot in Figure 3b. The Li|Li cells with both high- and medium-DMF electrolytes fail with open circuit. As we showed before<sup>[11]</sup> (and also see Figure S7), the Li|Li cell with a high-DMF electrolyte shows a long-term cycling stability of over 1000 hours against Li metal at  $0.2 \text{ mA cm}^{-2}$ , and fails with open circuit after 100 hours when the current density increases to  $0.35 \text{ mA cm}^{-2}$ . Thus the maximum applicable current density of the medium-DMF electrolyte for realizing a long-term cycling stability in the Li|Li cell should be above  $0.2 \text{ mA cm}^{-2}$ . The high-DMF electrolyte membrane in a disassembled cell after failure was found to be dark brown (Figure S8a). The brown color is caused by the dehydrofluorination of the PVDF as evidenced by the appearance of the C=C peak in the FTIR spectrum of the detached electrolyte membrane (Figure 3c), which coincides with the analysis in our previous work.<sup>[11]</sup> In the low-DMF case, the PVDF–LiFSI electrolytes with a much lower content of residual DMF do not show better cycling performance in the Li|Li cells (Figure 3d). By contrast, the Li|Li cell with the low-DMF electrolyte shows a larger voltage polarization than that with the high- or medium-DMF electrolytes (Figure S9) and, differently, fails with short circuit. The detached low-DMF electrolyte membrane after the cell failure remains semi-transparent (Figure S8b), implying no occurrence of the dehydrofluorination of PVDF. The PVDF–LiFSI electrolytes with different contents of residual DMF also have different electrochemical stability windows as shown in Figure 3e. With the applied voltage increasing at a rate of  $0.1 \text{ mV s}^{-1}$ , the current signal for a high-DMF case arises at 3.8 V. In the range of 3.8–4.5 V, the current slowly increases and then decreases to form a

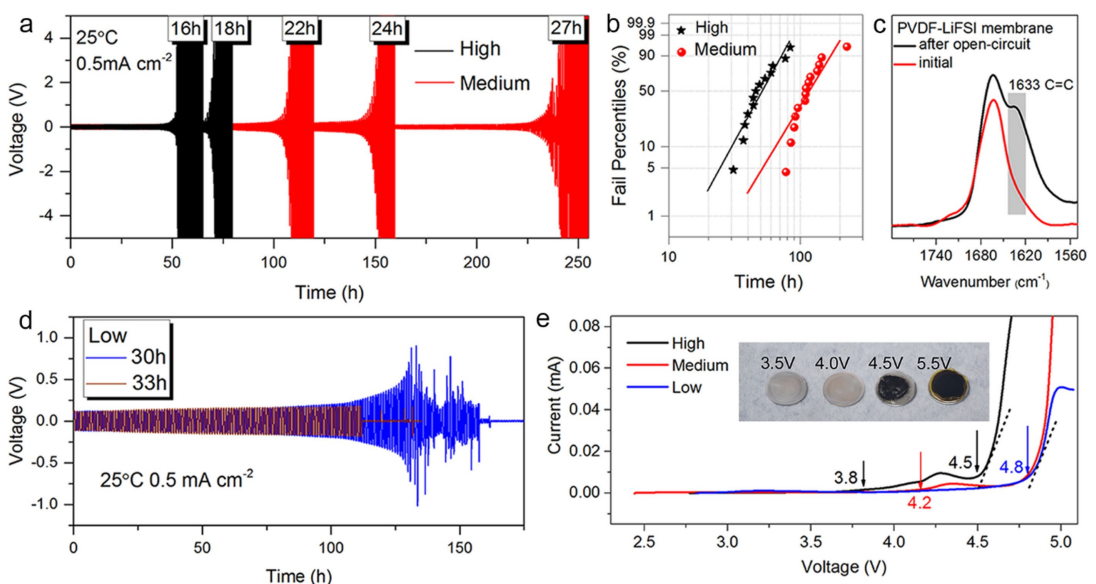


**Figure 3.** Effects of residual DMF on electrochemical stability of PVDF–LiFSI electrolytes. a) Galvanostatic cycling profiles of Li|PVDF–LiFSI electrolyte|Li cells. The electrolytes with vacuum drying for 16&18 h and 22&24&27 h fall into the categories of high-DMF and medium-DMF electrolytes, respectively. b) Weibull distribution of failure time. Failure time denotes the time when the voltage of the Li|Li cell reaches 4 times of the initial value. c) FTIR spectra of the PVDF–LiFSI membrane with high DMF content before the Li|Li cycling test and after open-circuit of the Li|Li cell. d) Galvanostatic cycling profiles of Li|PVDF–LiFSI electrolyte|Li cells, where the electrolytes with vacuum drying for 30&33 h belong to the category of low-DMF electrolytes. e) CV curves of pure PVDF, and high-, medium- and low-DMF electrolytes. Inset: photo images of the detached high-DMF electrolyte membranes after 3.5, 4.0, 4.5 and 5.5 V testing.

small hump. After 4.5 V and beyond, the current rises rapidly. The high-DMF electrolyte membrane maintains its native color at 3.5 V, exhibits minimal yellowing at 4.0 V, and presents distinct dark brown at 4.5 and 5.5 V (see the inset in Figure 3e). Therefore, the decomposition of the high-DMF electrolyte starts at 3.8 V and accelerates above 4.5 V. With the decrease of the DMF residue in the electrolyte, the electrochemical stability of the PVDF–LiFSI electrolyte is remarkably enhanced. For example, the decomposition of a medium-DMF electrolyte begins at 4.2 V and a low-DMF electrolyte can be stable up to 4.8 V with no obvious current fluctuation.

As discussed in our previous work,<sup>[11,12]</sup> when a PVDF–LiFSI electrolyte is contacted with Li metal, the decomposition of LiFSI causes the formation of a LiF-rich mosaic interface layer, which is beneficial to the stable cycling of the Li|Li cell. However, at a large current density, the continuous reactions between the electrolyte and a Li anode could result in the decomposition of the electrolyte and the propagation of the interface, thus leading to the failure of the Li|Li cells. Our experiments show that DMF plays an important role in the interfacial reactions, as seen from Notes S2–3 for details. The reaction between DMF and Li metal is actually associated with the N=C=O group in DMF as discussed in Note S3 and is supposed to be caused by the exchange and transfer of electrons. To trace the electron behavior between DMF and Li metal, the charge density difference plots were obtained by first-principles calculations and presented in Figure 4a and Figure S14. When DMF is directly absorbed on a Li foil, the

accumulation of electrons around the C atom and the charge depletion around the N atom reveal that the C–N bonds in DMF is likely to be broken. In addition, electrophilic attack of •OH also can facilitate the cleavage of the C–N bonds in DMF in an alkaline environment created by the co-existence of Li metal and minimum H<sub>2</sub>O.<sup>[21]</sup> Accordingly, we conclude that DMF could be initially decomposed into •CH<sub>2</sub>N(CH<sub>3</sub>)COH free radical and further decomposed into other free radicals such as •N(CH<sub>3</sub>)<sub>2</sub>, •CHO and •CH<sub>3</sub> with the C–N bond cleavage, which is similar to the decomposition process in previous studies on photo-decomposition of DMF.<sup>[21,22]</sup> This conclusion can be further confirmed by the two facts, i.e., first, when the pure DMF solvent is directly dripped onto a Li foil, H<sub>2</sub>, NH<sub>3</sub>, HCHO and HN(CH<sub>3</sub>)<sub>2</sub> are generated as displayed in Figure 4b. C–N, C=O, C–O and amine/amide peaks are detected on the surface of the Li foil after the reaction with DMF solution by X-ray photoelectron spectroscopy (XPS) (Figure 4c) and Raman spectroscopy (Figure S15). These detected gases and chemical species on the Li foil are generated from the free radical reactions; second, in the PVDF–LiFSI–DMF solution with a Li foil immersed in, we indeed detected the existence of •CH<sub>3</sub>, •OH and •CH<sub>2</sub>(CH<sub>3</sub>)NCOH free radicals by electron paramagnetic resonance (EPR) as shown in Figure 4d.

Based on the analysis above, a failure mechanism of the interface between the PVDF-based electrolyte and a Li anode is proposed. As illustrated in Figure 4e, electron transfer between DMF and a Li foil results in the generation of free radicals such as •N(CH<sub>3</sub>)<sub>2</sub>, •CHO and •CH<sub>3</sub> as aforementioned. Under the

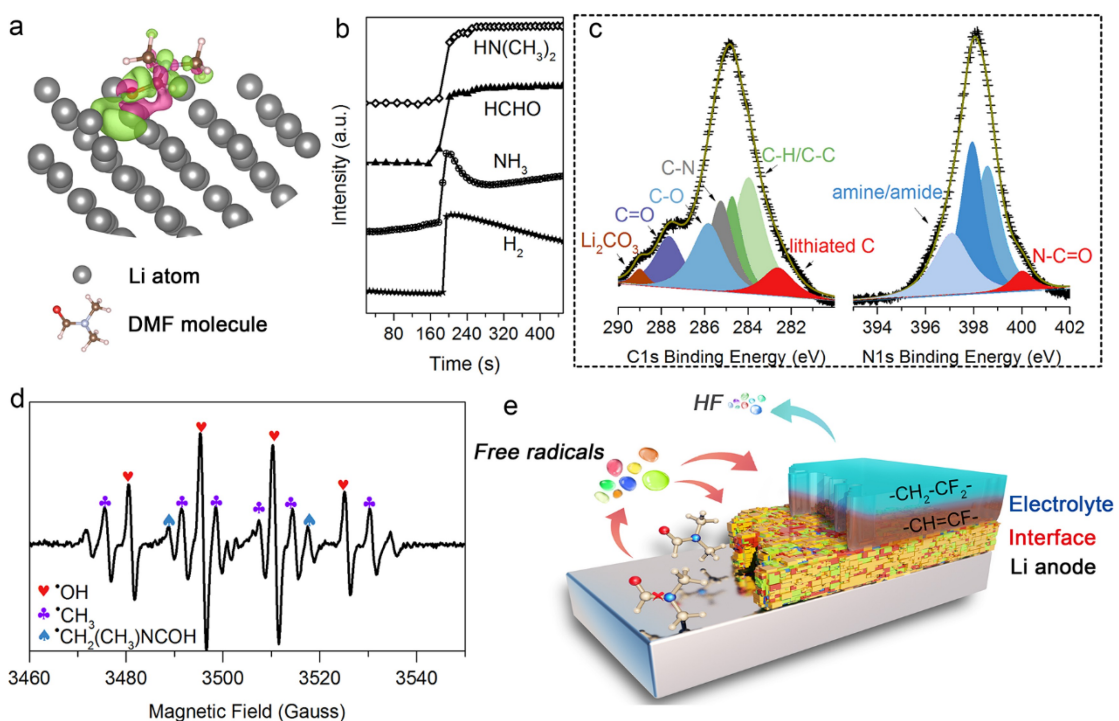


**Figure 4.** Role of DMF in the interfacial reaction in the PVDF-based system. a) Computed charge density difference of DMF-absorbed Li(001). The red and green isosurfaces represent charge accumulation and depletion in the space, respectively. The isovalue is 0.0015 au. b) Gas evolution profiles indicate the generation of H<sub>2</sub>, NH<sub>3</sub>, HCHO and HN(CH<sub>3</sub>)<sub>2</sub> during the reaction between Li metal and pure DMF solvent. c) XPS spectra of a Li foil after the reaction with pure DMF solvent. d) EPR spectrum of the PVDF–LiFSI–DMF solution after the reaction with a Li foil. e) Schematic diagram of the failure mechanism at the interface between the PVDF–LiFSI electrolyte and a Li metal anode.

attack of these free radicals, PVDF can be dehydrofluorinated with the formation of conjugated  $-\text{CH}=\text{CF}-$  double bonds and the generation of HF. Some chemical species can also be formed between the electrolyte and Li metal with the radical reactions, leading to the propagation of the interface layer. The decomposed electrolyte and thickened interface finally cause a large impedance and thus the open circuit of the  $\text{Li}|\text{Li}$  cell. Next, let us concretely discuss the failure in high-, medium- and low-DMF cases during the  $\text{Li}|\text{Li}$  cycling. DMF is more likely to generate free radicals in the high-DMF case in comparison with the medium case, which thus induces the decomposition of the electrolyte and the formation of the inert interface. The medium-DMF electrolyte with a relatively low amount of DMF hence shows better cycling performance in a  $\text{Li}|\text{Li}$  cell compared to the high-DMF one. In the low-DMF case, it is difficult to trigger the continuous interfacial reaction with a small amount of DMF. In consequence, the low-DMF electrolyte exhibits no open-circuit feature in the  $\text{Li}|\text{Li}$  cell and fails with short circuit as in PEO-based electrolytes, which is caused by the Li dendrites that penetrate through the electrolytes.

Finally, we investigated the effect of DMF residue on the cycling performance of the full cells with the PVDF-based electrolytes. All of the full cells were operated at 25 °C. Figure 5a shows a comparison of the cycling performance of the solid-state  $\text{LiFePO}_4|\text{Li}$  cells assembled with the high-, medium- and low-DMF electrolytes. The  $\text{LiFePO}_4|\text{Li}$  cells were galvanostatically cycled between 2.7 and 4.0 V. For the high- and medium-DMF cases, the high ionic conductivity of the electrolytes and good interfacial contact between the electro-

des and the electrolyte lead to a low cell resistance (see the inset in Figure 5a). The  $\text{LiFePO}_4|\text{Li}$  cells hence deliver a high discharge capacities of  $\sim 142 \text{ mAh g}^{-1}$  during the first 30 cycles when the high- and medium-DMF electrolytes are used. However, the discharge capacity of the cell with the high-DMF electrolyte gradually decreases with the increase of the cycle number and is significantly lower than that of the cell with the medium-DMF electrolyte after hundreds of cycles. The capacity fade in the high-DMF case is mainly ascribed to the low electrochemical window and poor stability of the electrolyte against the Li anode as discussed above. In the low-DMF case, the low ionic conductivity of the electrolyte and high interfacial impedance between the electrodes and the electrolyte induce a large polarization and thus a rapid decay of the cell. Obviously, the cell with the medium-DMF electrolyte shows the best cycling performance of over 1000 cycles with a capacity retention of 94% at 0.35 C (here, the capacity retention is defined as the ratio of the capacity at the last cycle to the highest capacity during cycling). Furthermore, Figure 5b shows that the solid-state  $\text{LiFePO}_4|\text{medium-electrolyte}|\text{Li}$  cell possess a high capacity retention of 90% after 600 cycles even at 0.7 C. The  $\text{NCM}|\text{medium-electrolyte}|\text{Li}$  cell, which is cycled between 3.0 and 4.2 V at 0.5 C, also shows a good performance of over 600 cycles with a capacity retention of 92% (Figure 5c). The superior long-term cycling stability benefits from the high ionic conductivity and excellent electrochemical stability of the medium-DMF electrolyte.

In summary, we have systematically investigated the role of DMF in the PVDF-based electrolytes with a residual DMF

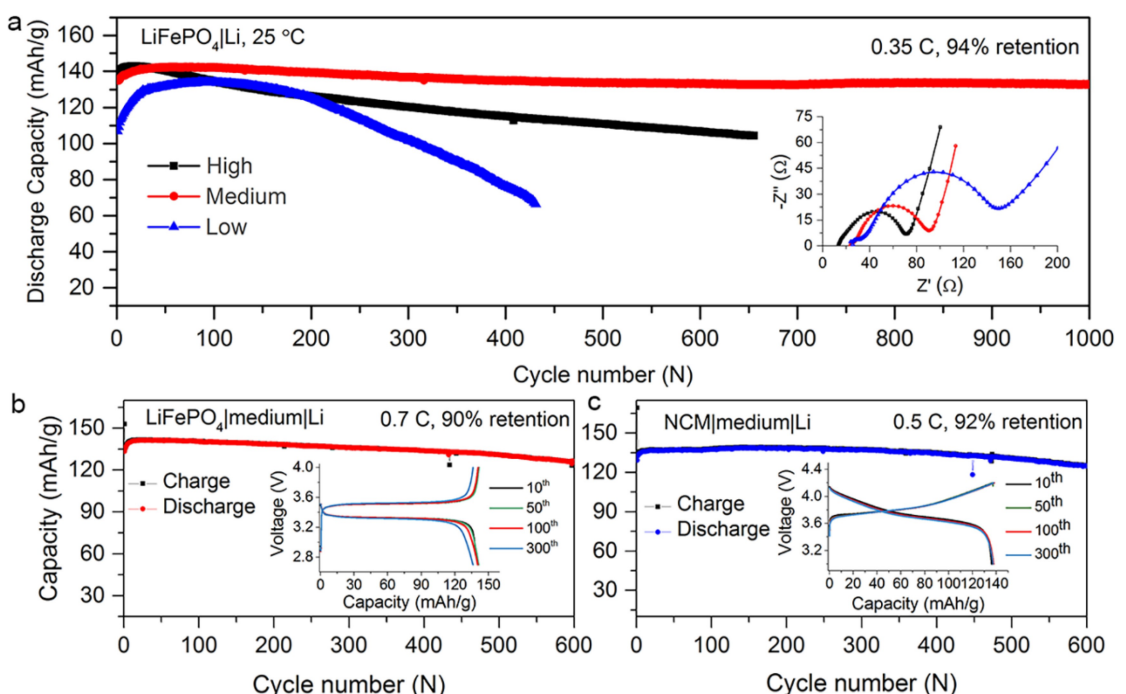


**Figure 5.** Cycling performance of full cells with PVDF–LiFSI electrolytes at 25 °C. a) Comparison of the cycling performance of  $\text{LiFePO}_4|\text{Li}$  cells with high-, medium- and low-DMF electrolytes at 0.35 C. Inset: impedance spectra of the  $\text{LiFePO}_4|\text{Li}$  cells before cycling. Cycling performance of b) the  $\text{LiFePO}_4|\text{Li}$  cell with a medium-DMF electrolyte at 0.7 C and c) the  $\text{NCM}|\text{Li}$  cell with a medium-DMF electrolyte at 0.5 C. Insets: corresponding charge-discharge curves of the  $\text{LiFePO}_4|\text{Li}$  and  $\text{NCM}|\text{Li}$  cells.

content of 5–17 wt%. The residual DMF molecules in the electrolytes are complexed with Li ions to form  $[Li(DMF)]_x^+$  ( $x \leq 3.29$ ) and there is no free DMF solvent.  $Li^+$  is transported among the interaction sites between  $[Li(DMF)]_x^+$  and the PVDF chains. At the same time, the bound DMF residue also affects the electrochemical stability of the electrolytes. The solvation effect in the PVDF–LiFSI electrolyte can be optimized by tuning the amount of residual DMF to an appropriate range (e.g., 10–14 wt%); therefore, the PVDF–LiFSI electrolyte can be controlled to possess the optimal overall performance such as high ionic conductivity, wide electrochemical window and excellent stability against a Li anode. The full cells with the optimized PVDF–LiFSI electrolyte hence present significantly improved long-term cycling stability at room temperature. Specifically, the solid-state  $LiFePO_4$ –Li cells deliver high capacity retentions of 94% and 90% after 1000 cycles at 0.35 C and 600 cycles at 0.7 C, respectively. The NCM|Li cell shows a stable cycling life of more than 600 cycles with a capacity retention of 92%. The fundamental understanding of the electrochemistry/chemistry reactions in the PVDF-based electrolytes enables the significant improvement of the electrochemical performance of the electrolytes and thus promotes the development of high-energy-density and high-safety Li metal batteries.

## Experimental Section

### Synthesis

PVDF (Arkema, Kynar 761) and LiFSI (Tinci Materials Technology Co., Ltd, China) were dried in vacuum at 80 °C for 24 h before use. PVDF–LiFSI (3:2 in weight ratio) electrolyte membranes were prepared by the conventional solution-casting method as reported before.<sup>[11,12]</sup> Different solvents including DMF, DMAc, NMP and a THF-DMF mixture (7:3 in volume ratio) were used. The casted electrolyte membranes were dried in a vacuum oven to remove the solvent. The electrolyte membranes with different contents of DMF residue were obtained by adjusting the drying time under vacuum. The high-DMF electrolytes were obtained by drying at 80 °C for 15–20 h; the medium-DMF electrolytes were obtained by drying for 21–28 h at 80 °C; the low-DMF electrolytes were obtained by drying for 29–40 h at 80 °C or by first drying at 80 °C for 24 h and then baking at 100 °C for 2–6 h. The membranes prepared with *N,N*-dimethylacetamide (DMAc) or *N*-methyl-2-pyrrolidone (NMP) were dried in vacuum at 90 °C for 18–35 h.

### Electrochemistry

The ionic conductivity was measured using a Zahner-elektrik IM6 analyzer by assembling the electrolyte membrane into a symmetric stainless steel (SS) cell, SS|electrolyte|SS. The activation energy  $E_a$  was calculated according to the Arrhenius equation  $\sigma(T) = A \exp(-E_a/RT)$ , where  $\sigma$  was the ionic conductivity,  $T$  was absolute temperature, and  $A$  was a pre-exponential factor. The electrochemical stability window of the electrolyte was determined by the cyclic voltammetry (CV) test, which was carried out on a Bio-Logic SAS VMP3 workstation at a scanning rate of 0.1 mVs<sup>-1</sup>. Two kinds of composite cathodes were prepared and matched with the as-prepared PVDF–LiFSI electrolytes and Li anode to assemble full cells. One was the mixture of battery-grade  $LiFePO_4$  powder, PEO ( $M_w \sim 600\,000$ ), super-P and LiTFSI (Sigma-Aldrich) (w:w:w:w=

75:11:10:4) with a  $LiFePO_4$  active material loading of ~1.7 mg cm<sup>-2</sup>. The other was the mixture of battery-grade  $LiNi_{0.6}Co_{0.2}Mn_{0.2}O_2$  (NCM622) powder, PEO, super-P and LiTFSI (w:w:w:w=76:10:4:10) with a NCM active material loading of ~2.6 mg cm<sup>-2</sup>. All of Li|Li symmetric cells and full cells were assembled using CR2025-type coin cells in an Ar-filled glove box and the cycling test of these cells was performed with LAND systems.

### Characterization

The TGA test was carried out with  $N_2$  flowing over the samples heated at a rate of 10 °C min<sup>-1</sup> with a Waters-Discovery instrument. Solid-state <sup>13</sup>C NMR data were acquired using a JNM-ECZ600R spectrometer. FTIR spectra were recorded on a VERTEX 70 spectrometer. Nano-IR measurements were undertaken with a Bruker Anasys nanoIR3 instrument. To prepare a testing sample, a homogeneous PVDF–LiFSI–DMF solution was dripped on a 1 cm × 1 cm glass substrate and then dried in vacuum at 80 °C for 15 h. DSC was conducted using a thermal analysis apparatus (Q5000IR, TA instruments) with a heating/cooling ramp of 10 °C min<sup>-1</sup> from 25 to 200 °C under Ar atmosphere. The crystallinity of PVDF  $X_c$  was calculated by the equation  $X_c = ((\Delta H_f/\omega)/\Delta H_f^*) \times 100\%$ , where  $\Delta H_f^*$  was the melting enthalpy of 100% crystalline PVDF and was 104.5 J g<sup>-1</sup>,  $\Delta H_f$  was the melting enthalpy of the membranes measured in DSC, and  $\omega$  is the weight fraction of PVDF in the PVDF-based electrolyte membranes.<sup>[23]</sup> XRD patterns were collected on a Rigaku D/max-2500 (Cu–K $\alpha$ ) diffractometer. Ex-situ gas detection was carried out by a mass spectrometer (Hiden Analytical, HPR-20 R&D). The electron paramagnetic resonance (EPR) spectra were recorded by a Bruker E500 spectrometer at 95 K and 5,5-dimethylpyrroline-N-oxide (DMPO) was selected as the trapping agent. XPS was performed using a Thermo Scientific ESCALab 250Xi XPS system without exposure to air. Raman spectra were obtained with a Raman spectrometer (LabRAM HR Evolution).

### Computational method

First-principles calculations were performed in the Perdew-Burke-Ernzerhof (PBE) generalized gradient approximation (GGA), implemented in the Vienna Ab initio Simulation Package (VASP).<sup>[24]</sup> The projector augmented-wave (PAW) potentials were used for the treatment of the core electrons.<sup>[25]</sup> Kohn-Sham single electron wave functions were expanded in a plane-wave basis with a kinetic energy cutoff of 400 eV to describe the valence electrons. The Tkatchenko-Scheffler method was used to count for the long range dispersion corrections.<sup>[26]</sup> The Li–DMF complex was modeled as three DMF molecules coordinating around Li in a planar triangle geometry for simplicity. The interaction between the complex and the amorphous PVDF was approximated by placing the complex on the F side of a  $(CH_2CF_2)_{10}$  chain model since it was reported that  $N-CH_3$  in DMF can interact with PVDF chains.<sup>[18]</sup> To trace the electron behavior between DMF and a Li metal anode, three possible spatial conformations for DMF adsorbed on a Li(001) surface<sup>[27]</sup> were considered, i.e., DMF parallel to the Li(001) surface, DMF vertical to the Li(001) surface with  $CH_3-CH_3$  side close to Li and DMF vertical to the Li(001) surface with H-C=O side near the Li. A vacuum layer was set to be larger than 20 Å. The charge density difference was determined by  $\Delta\rho(r) = \rho_{AB}(r) - \rho_A(r) - \rho_B(r)$ ,<sup>[28]</sup> where  $\rho_A$ ,  $\rho_B$  and  $\rho_{AB}$  represented the charge densities of Li(001) individual system, DMF individual system and Li(001)–DMF composite system, respectively.

## Acknowledgements

This work was supported by Basic Science Center Program of National Natural Science Foundation of China (NSFC) under Grant No. 51788104, NSFC projects under Grant Nos. 51572149 and 51532002 and Tsinghua University Startup Fund.

## Conflict of Interest

The authors declare no conflict of interest.

**Keywords:** poly(vinylidene fluoride) • electrolytes • solvation effect • interface chemistry • solid-state lithium metal batteries

- [1] a) M. S. Whittingham, *Chem. Rev.* **2004**, *104*, 4271; b) B. Scrosati, J. Garche, *J. Power Sources* **2010**, *195*, 2419; c) F. Cheng, J. Liang, Z. Tao, J. Chen, *Adv. Mater.* **2011**, *23*, 1695.
- [2] J. B. Goodenough, K.-S. Park, *J. Am. Chem. Soc.* **2013**, *135*, 1167.
- [3] a) X. Liang, Q. Pang, I. R. Kochetkov, M. S. Sempere, H. Huang, X. Sun, L. F. Nazar, *Nat. Energy* **2017**, *2*, 17119; b) L. de Biasi, B. Shwarz, T. Brezesinski, P. Hartmann, J. Janek, H. Ehrenberg, *Adv. Mater.* **2019**, *31*, 1900985; c) D. Geng, N. Ding, T. S. A. Hor, S. W. Chien, Z. Liu, D. Wuu, X. Sun, Y. Zong, *Adv. Energy Mater.* **2016**, *6*, 1502164.
- [4] T. Bartsch, F. Strauss, T. Hatsukade, A. Schiele, A. Y. Kim, P. Hartmann, J. Janek, T. Brezesinski, *ACS Energy Lett.* **2018**, *3*, 2539.
- [5] N. Xu, T. Qian, X. Liu, J. Liu, Y. Chen, C. Yan, *Nano Lett.* **2017**, *17*, 538.
- [6] H. Guo, W. Luo, J. Chen, S. Chou, H. Liu, J. Wang, *Adv. Sustainable Syst.* **2018**, *2*, 1700183.
- [7] M. D. Tikekar, S. Choudhury, Z. Tu, L. A. Archer, *Nat. Energy* **2016**, *1*, 16114.
- [8] a) F. Croce, G. B. Appeticchi, L. Persi, B. Scrosati, *Nature* **1998**, *394*, 456; b) T. Fampricci, P. Canepa, J. A. Dawson, M. S. Islam, C. Masquelier, *Nat. Mater.* **2019**, *18*, 1278.
- [9] a) K. Fu, Y. Gong, J. Dai, A. Gong, X. Han, Y. Yao, C. Wang, Y. Wang, Y. Chen, C. Yan, Y. Li, E. D. Wachsman, L. Hu, *Proc. Mont. Acad. Sci.* **2016**, *113*, 7094; b) W. Liu, N. Liu, J. Sun, P.-C. Hsu, Y. Li, H.-W. Lee, Y. Cui, *Nano Lett.* **2015**, *15*, 2740; c) J. Zhang, J. Zhao, L. Yue, Q. Wang, J. Chai, Z. Liu, X. Zhou, H. Li, Y. Guo, G. Cui, L. Chen, *Adv. Energy Mater.* **2015**, *5*, 1501082.
- [10] a) F. Boudin, X. Andrieu, C. Jehoulet, I. I. Olsen, *J. Power Sources* **1999**, *81*–*82*, 804; b) S.-S. Choi, Y. S. Lee, C. W. Joo, S. G. Lee, J. K. Park, K.-S. Han, *Electrochim. Acta* **2004**, *50*, 339.
- [11] X. Zhang, S. Wang, C. Xue, C. Xin, Y. Lin, Y. Shen, L. Li, C.-W. Nan, *Adv. Mater.* **2019**, *31*, 1806082.
- [12] X. Zhang, T. Liu, S. Zhang, X. Huang, B. Xu, Y. Lin, B. Xu, L. Li, C.-W. Nan, Y. Shen, *J. Am. Chem. Soc.* **2017**, *139*, 13779.
- [13] P. Yao, B. Zhu, H. Zhai, X. Liao, Y. Zhu, W. Xu, Q. Cheng, C. Jayyosi, Z. Li, J. Zhu, K. M. Myers, X. Chen, Y. Yang, *Nano Lett.* **2018**, *18*, 6113.
- [14] B. Li, Q. Su, L. Yu, D. Wang, S. Ding, M. Zhang, G. Du, B. Xu, *ACS Appl. Mater. Interfaces* **2019**, *11*, 42206.
- [15] M. M. Heravi, M. Ghavidel, L. Mohammadkhani, *RSC Adv.* **2018**, *8*, 27832.
- [16] J. Lang, Y. Long, J. Qu, X. Luo, H. Wei, K. Huang, H. Zhang, L. Qi, Q. Zhang, Z. Li, H. Wu, *Energy Storage Mater.* **2019**, *16*, 85.
- [17] P. Martins, A. C. Lopes, S. Lanceros-Mendez, *Prog. Polym. Sci.* **2014**, *39*, 683.
- [18] M. M. E. Jacob, A. K. Arof, *Electrochim. Acta* **2000**, *45*, 1701.
- [19] a) Z. Wang, B. Huang, Z. Lu, S. Wang, R. Xue, L. Chen, *Solid State Ionics* **1996**, *92*, 265; b) K. Fujii, H. Wakamatsu, Y. Todorov, N. Yoshimoto, M. Morita, *J. Phys. Chem. C* **2016**, *120*, 17196.
- [20] M. A. Ratner, D. F. Shriver, *Chem. Rev.* **1988**, *88*, 109.
- [21] M. Klare, J. Scheen, K. Vogelsang, H. Jacobs, J. A. C. Broekaert, *Chemosphere* **2000**, *41*, 353.
- [22] a) X. Feng, Z. Li, *J. Photochem. Photobiol. A* **2017**, *337*, 19; b) C. L. Øpstad, T.-B. Melø, H.-R. Sliwka, V. Partali, *Tetrahedron* **2009**, *65*, 7616.
- [23] W. Ma, J. Zhang, X. Wang, S. Wang, *Appl. Surf. Sci.* **2007**, *253*, 8377.
- [24] a) G. Kresse, J. Furthmüller, *Phys. Rev. B* **1996**, *54*, 11169; b) J. P. Perdew, K. Burke, M. Ernzerhof, *Phys. Rev. Lett.* **1996**, *77*, 3865.
- [25] G. Kresse, D. Joubert, *Phys. Rev. B* **1999**, *59*, 1758.
- [26] A. Tkatchenko, M. Scheffler, *Phys. Rev. Lett.* **2009**, *102*, 073005.
- [27] Z. Liu, Y. Qi, Y. X. Lin, L. Chen, P. Lu, L. Q. Chen, *J. Electrochem. Soc.* **2016**, *163*, A592.
- [28] C. Hobbs, L. Kantorovich, J. D. Gale, *Surf. Sci.* **2005**, *591*, 45.

Manuscript received: April 9, 2020

Revised manuscript received: April 27, 2020

Version of record online: May 13, 2020